Electronic Supplementary Material (ESI) for Chemical Communications.
This journal is © The Royal Society of Chemistry 2017

Towards well-defined MoS_2 nanoribbons on a large scale

Ruifeng Qi[a], Shanling Wang[b], Minxiang Wang[c], ,Wentao Liu[a], Zhihui Yan[a], Xiaofeng Bi[a], Qingsong Huang[a]*

[a]School of Chemical Engineering , Sichuan University, Chengdu 610065, China.
[b]Analysis and test center, Sichuan University, Chengdu 610065, China.
[c]State Key Laboratory of Surface Physics, Department of Physics, and Laboratory of Advanced Materials, Fudan University, Shanghai 200433, China.

1. TEM images of MNRs growth process

Fig. S1 (a-b) the TEM images of MoO_3 (as-received). The molybdenum trioxide film consists of several sub-layers. Fig. S1 (c) (d) is MoO_2. After annealing at 500 ^oC, some of the edge facets are blank (Fig. S1(c)).

Fig. S1 (d-f) refer to MNRs@MoO_2. After annealing at 750 ^oC, the majority of MoS_2 nanoribbons concentrated within 10 layers. Fig. S1 (g) show the reference sample annealing at 1000 ℃, which is obtained by raising the temperature of the second step to 1000 ℃. Almost all of the small pieces of the sample has been completely converted to molybdenum disulfide as shown in Fig. S1 (g).

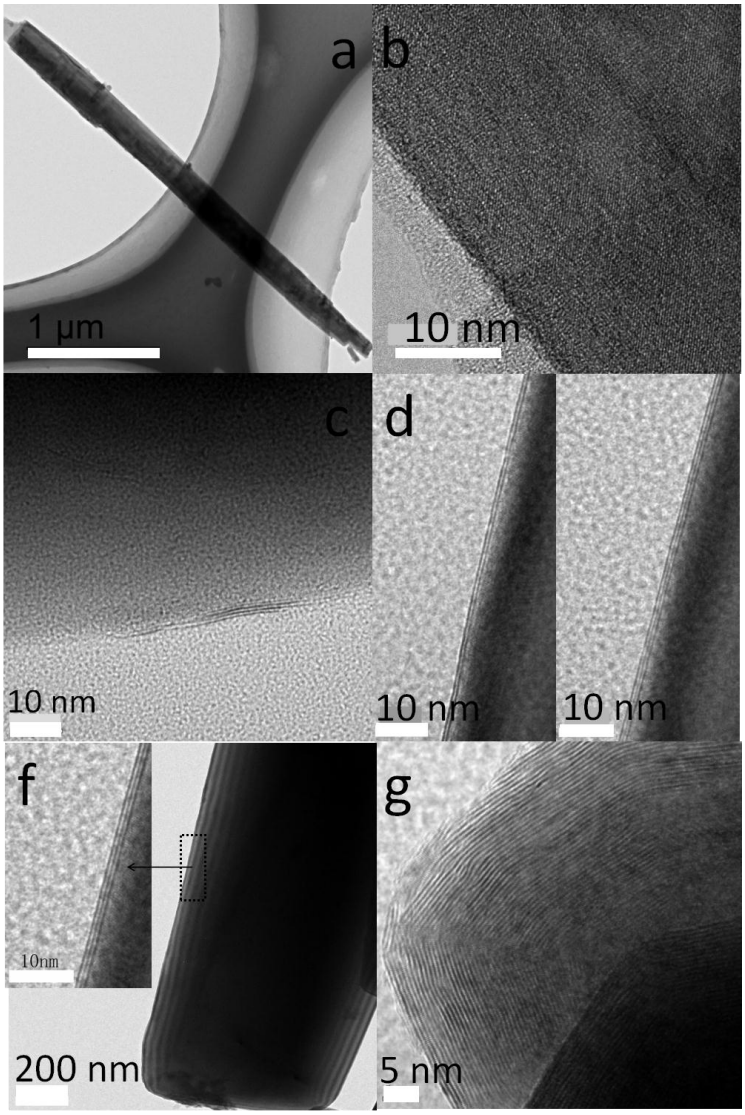

Fig. S1 TEM images (a-b) MoO_3 (as-received), (c)MoS_2@MoO_2 (annealing at 500 ^oC), (d-f) MNRs@MoO_2 (annealing at 750^oC) and (g) MoS_2@MoO_2 (annealing at 1000^oC).

2. Morphologies of MNRs growth process

Fig. S2 (a-b) show the optical microscope images of molybdenum trioxide. The molybdenum trioxide layer consists of several sub-layers, stacked into steps. Fig. S2 (c-d) are the SEM images of freshly obtained MoS_2@MoO_2. After annealing around 500 ^oC, most part of molybdenum trioxide is converted into molybdenum dioxide. The middle part of MoO_3 is kept from changing against the freshly obtained MoO_2, mimicking a blooming flower as shown in Fig. (c-d). Fig. S2 (e-f) are the MNRs@MoO_2. Fig. S2 (g-h) is an SEM image of a reference sample obtained by raising the temperature in second step to 1000 ℃.

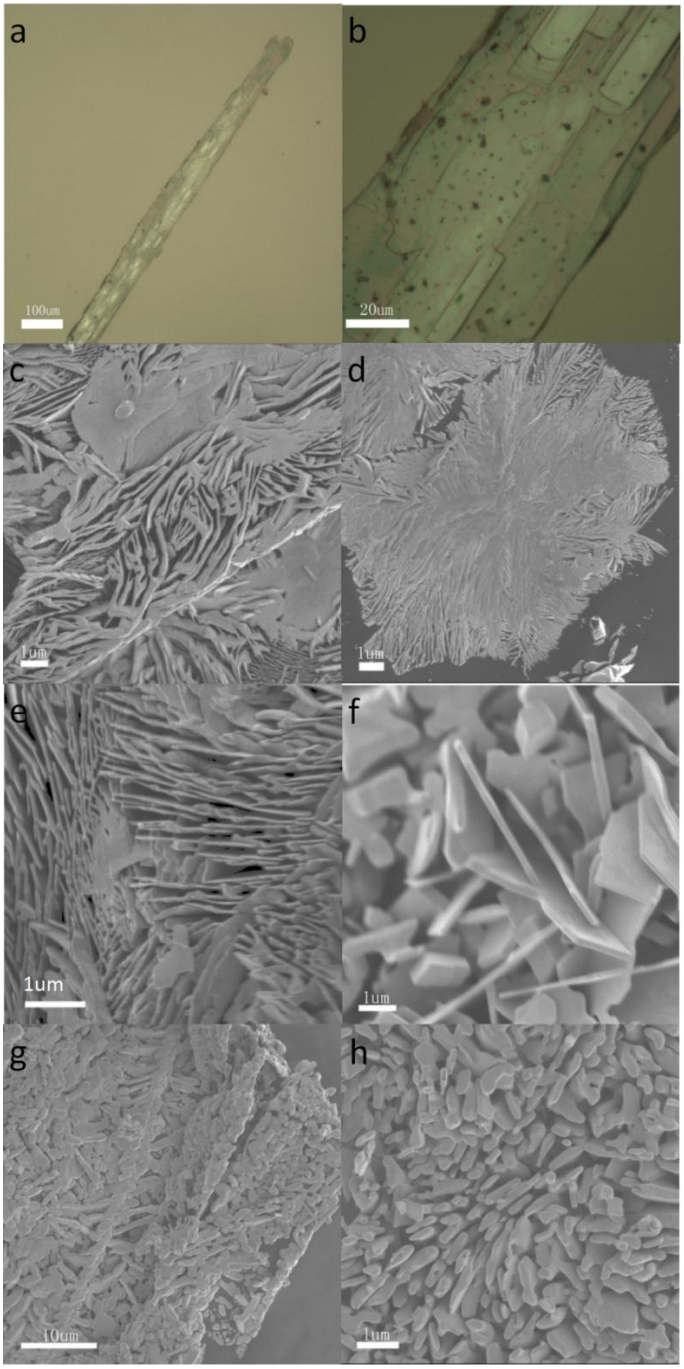

Fig. S2 (a-b) optical microscope images of the MoO_3 (as-received), (c-d) MoS_2@MoO_2 (annealing at 500 ^oC), (e-f) MNRs@MoO_2 (annealing at 750 ^oC), (g-h) the reference sample MoS_2@MoO_2 (annealing at 1000 ^oC).

3. Materials and Experiments

(1) The synthesis route for MoO_3

The Mo plate (99.9%, 17 mm*17 mm*1mm) purchasing from Chengdu KELONG Co. Ltd, was loaded in an alumina crucible, mounting an electrical-magnetism induction furnace. When the temperature was raised over 1900 ^oC, the Mo vapor reacted with oxygen in air and formed MoO_3nanobelts.

(2) Synthesis of MNRs@MoO_2

Molybdenum trioxide (100 mg) and sulfur (1 g, 99.9%, Chengdu KELONG Co. Ltd) were placed in a two-zone tubular furnace as shown in Fig. S3(a). The temperature of sulfur regions set at 300^{o}C, the temperature of molybdenum trioxide regions set at 500^{o}C (AL-500). The argon flow rate was maintained at 100 SCCM, reacting for 30min. After the two-zone tube dropped to room temperature, sulfur (1 g) was reloaded again, and successively the temperature rose to 300 ^{o}C. The temperature of molybdenum trioxide zone was raised to 750 ^{o}C (AL-750) correspondingly, sustaining argon flow 100 SCCM for 30min. After 30min reaction, the molybdenum disulfide nanoribbons were obtained. The temperature curve for MoO_3 section in the tube furnace is shown in Fig. S3(b). Fig. S3(c) demonstrates the photo of MNRs@MoO_2, resulting from AL-750. The total mass of the powder as photo is around 0.1 g.

(3) Characterization of zzMNRs@MoO_2

Raman spectroscopy (HORIBA) was used to study the structure symmetry and thickness of MoO_3, MoO_2 and zzMNRs@MoO_2 at 632.8 nm laser excitation. XRD (EMPYREAN) was employed to study the crystal structure of the samples. XPS (Kratos) was used to study components and valence states. SEM (JSM-7500F) was applied to check the morphology of samples. HRTEM was employed to study the morphology, crystal structure, and thickness of the zzMNRs@MoO_2 samples, performing on a FEI (Tecnai G2 F20 S-TWIN) at 200 kV. As for the zigzag edge states, a HRTEM was performed by FEI titan themis200TEM, whereas the EDS by Bruker super-XEDS, and EELS line scanning by 977Enfinium-EREELS. Fluorescence Spectrometer (F-7000) was adopted to explore the photoluminescence of the samples, and UV-Vis (UV-2100) for the band gap. The magnetic properties were characterized using a vibrating sample magnetometer (VSM, Quantum Design).

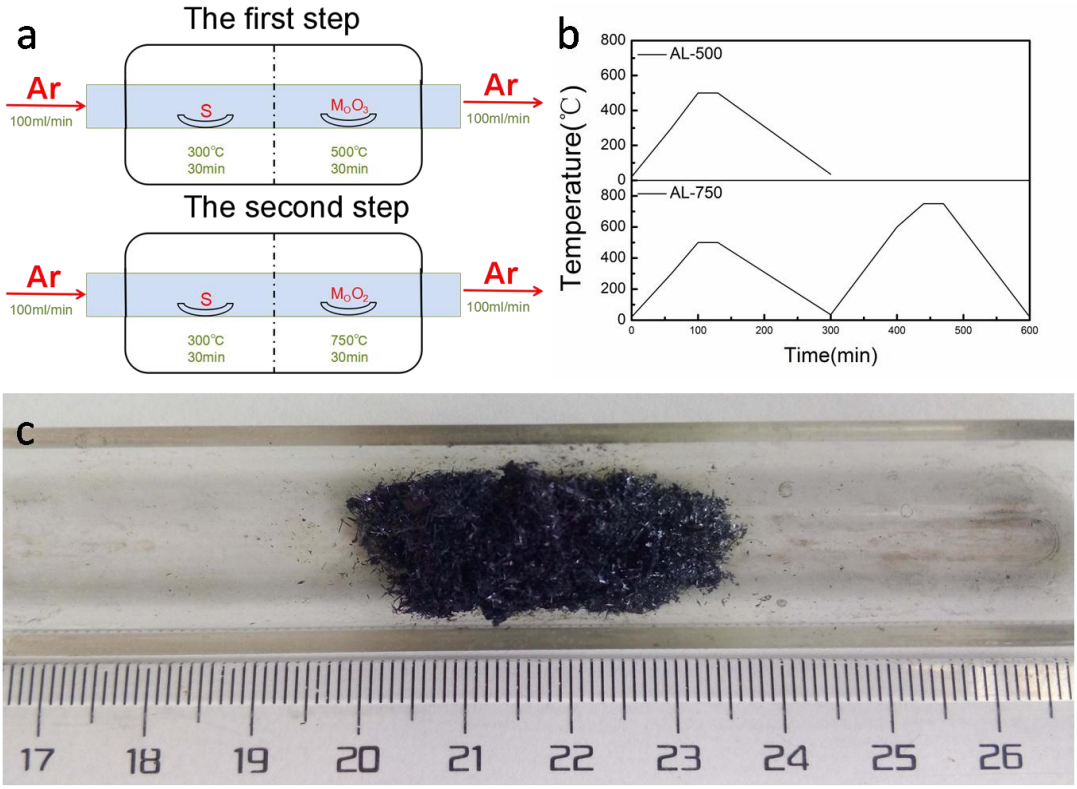

Fig. S3 (a) Schematic diagram of the MoS_2 growth process, (b) Temperature for MoS_2 growth, (c) MNRs@MoO_2 powder in the quartz boat.

4. Different annealing time at 750 °C

We performed the AL-750 with annealing time for 10 min (AL-750-S) and 50 min (AL-750-L) respectively. When annealing 10 min, the Raman frequency difference ($\Delta\omega$) between the out of plane A_{1g} mode, and in-plane E^1_{2g} mode is around 24 cm^{-1} (Fig. S4(a)), conforming to 2-4 layers[1-3]. The HRTEM has demonstrated a same result (Fig. S4(c)). Although the layer number was controlled very well, the MNRs were not fully extended, and quite few of side facets were left blank. As for annealing 50 min, $\Delta\omega$ is around 27 cm^{-1} (Fig. S4(b)), suggesting the MNR layer number is more than 6 layers[1-3], which has been confirmed by HRTEM (Fig. S4(d)). As a result, the annealing time has played an important role in controlling the layer number. When time was elongated, the MNR extending along edge sides and thickness increasing proceeded simultaneously.

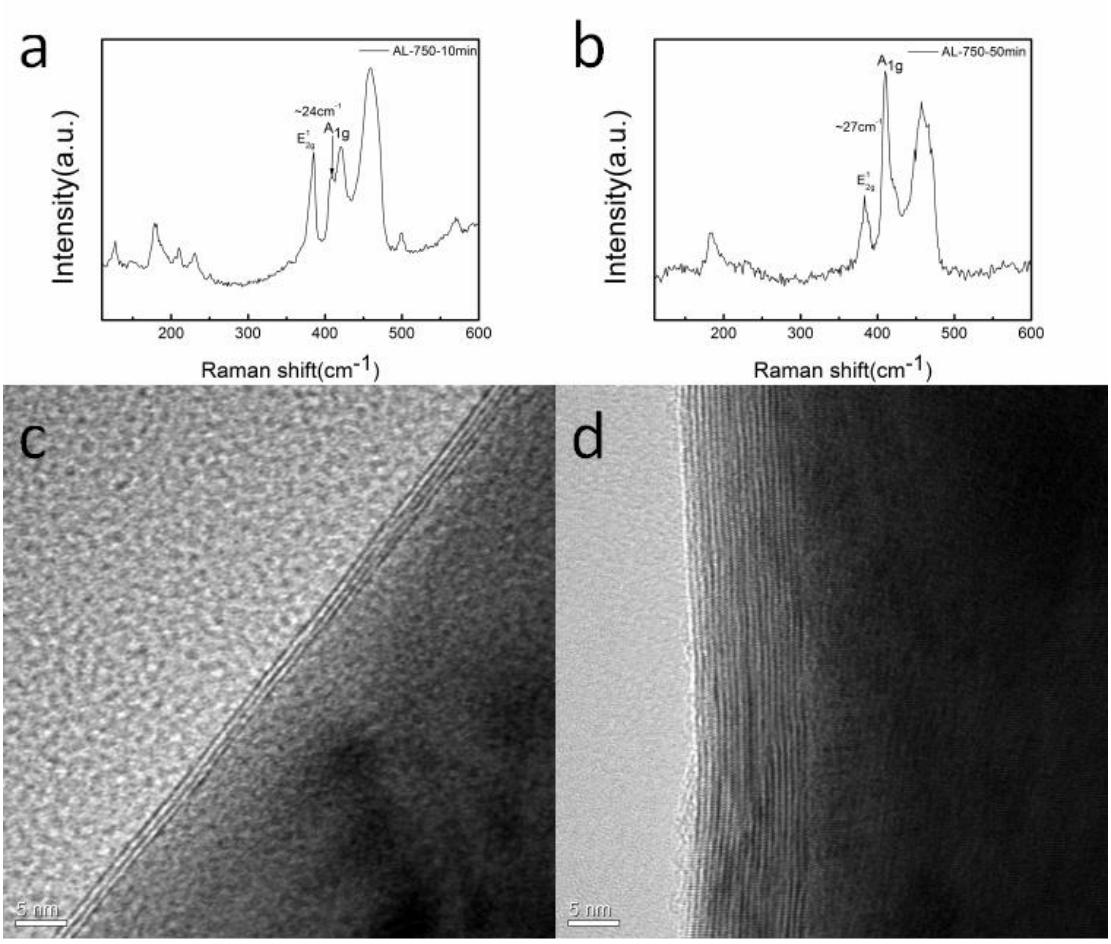

Fig. S4 The MNRs@MoO_2 arising from AL-750 with annealing time (a)(c) 10 min and (b)(d) 50 min.

5. Three kinds of situations for sulphur adding in one step.

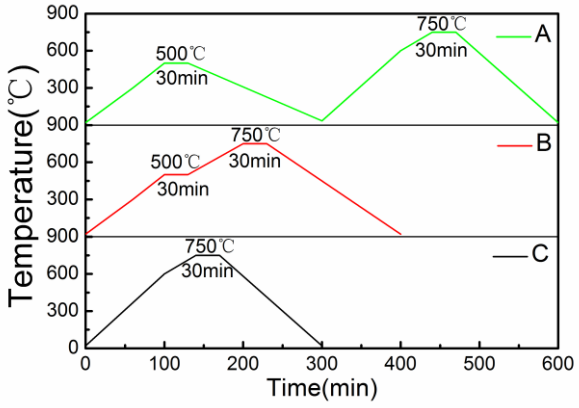

Fig.S5 Three kinds of situations for sulphur adding in one step. (A) the annealing process underwent two stages of heating-maintaining-cooling (HMC). (B) Heating to 500 °C, maintaining for 30 min, and heating directly to 750 °C. (C) Heating to 750 °C directly, adopting a slower heating rate when approaching the 750 °C than that in the initial stage.

(1) If "A" process is adopted (Fig. S5A), a large amount of sulfur should be added before initial step. Otherwise, the S vapor should become exhausted before the

experiment accomplished. If a large enough volume sulfur is added, the overflow of S flux would become condensation on the surface of the samples when the cooling stage after 500 ^{o}C maintenance, preventing the MNRs from forming. As a result, the "B" route is engineered to overcome the shortcomings.

(2) If "B" route is adopted (Fig. S5B), the temperature will be increased to 750 ^{o}C directly after 500 ^{o}C maintenance. The MNRs might be prepared via "B" route. However, in practice, several times sulphur mass are required to sustain the essential reaction time. Meanwhile, the long time heating make the sample-zone influence the S-zone in the tubular furnace, promoting the S-zone beyond the setting temperature gradually, so that S vapor flux become very huge, so that the S pressure in the sample area (reaction area) increased with the accumulative flux, resulting the nucleation and growth of MoS_2 become uncontrollable.

(3) If "C" route is adopted (Fig. S5C), most of the molybdenum trioxide underwent sublimated very quickly, because of the melting point 795 ^{o}C of molybdenum trioxide. When we performed the experiment according to "C" route, only very small amount samples were left in the quartz boat after 30 min annealing.

6. Specific growth mechanism for MNRs@MoO_2

Molybdenum trioxide (100 mg, synthesis method referring to Fig. S3) and sulfur powder (1 g, Chengdu Kelong Co.Ltd) were loaded in a quartz boat and placed in a two-zone tubular furnace. The temperature of sulfur zone was set at 300 ^{o}C, whereas the temperature of molybdenum trioxide zone was set around 500 ^{o}C. The argon flow rate was kept around 100 SCCM, annealing for 30 min. The process is named as AL-500. After the two-zone tube dropped to room temperature, sulfur (1 g) was reloaded, and raised to 300 ^{o}C successively. The temperature of molybdenum trioxide zone was raised to 750 ^{o}C (or 1000 ^{o}C) simultaneously, annealing in argon flow 100 SCCM for 10 min, 30 min and 50 min respectively. The process with annealing 30 min is named as AL-750 (or AL-1000).The process with annealing for 10 min (AL-750-S) or 50 min (AL-750-L) is just engineered for optimizing MNR growth time (Fig. S4). Finally, the zzMNRs@MoO_2 was obtained. The sulphur was loaded twice to optimize MNRs' quality and make synthesis process controllable (Fig. S5). Further information can be found in the supplementary information (Fig. S3, Fig. S6).

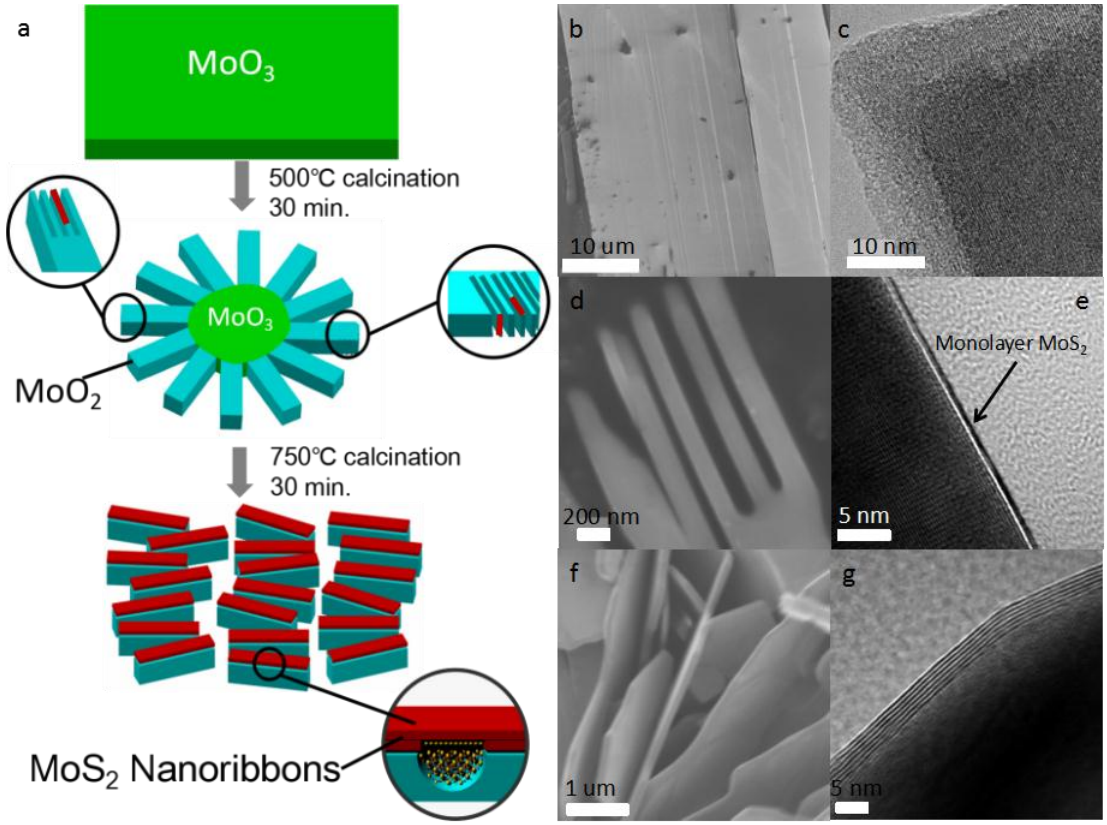

Fig. S6 (a) Schematic diagram of the reaction process, the reaction process can be classified into two steps. The MoO_3 single crystal nanobelt was cut along radial direction from rim to the center. Meanwhile, monolayer MoS_2 can form on the specific edge facets of the MoO_2 plates (inset in middle circle). On the occasion of 750 ^{o}C, the monolayer MNRs can develop into multilayers (inset in bottom circle), and extend to bare edge of substrate. (b)(c)SEM and HRTEM images of the MoO_3 nanobelt, as the raw MoO_3 nanobelt are stacked by several sub-layers. (d) MoO_2 is cut under 500 ^{o}C. (e) TEM images of the MoO_2 via AL-500. (f) SEM and TEM images of the MNRs@MoO_2 under 750 ^{o}C. The MoO_2 substrate was cut further into even thinner slab than that at 500 ^{o}C. (g) Monolayer MNRs developed into multilayers.

7. Why MNRs grow only along the side facets of the MoO_2 plates

The sulfur vapor should be probable to react with oxygen radical. Meanwhile, the sulphur might replace the oxygen radical, reconstructing into MoS_2 topologies.

Here the main surfaces of MoO_2 plates are {010} plane (Fig. S7(a)), whereas the orientation of side facets are mainly normal to zone axis [010]. Some defect facets (Fig. S7(c)), e.g. {101} facets, are usually available. Figure 1a shows that the S atoms are difficult to replace the O element, masked by Mo layers in the {010} main surface. Whereas the O elements are easier to be replaced by the S vapor in any side facets

(Fig. S7(b-c)) than those in {010} facets.

In addition, the corner and side small facets are usually influenced by the rim edge or ridge of the plates, where the Gibbs-Thomson effect has played an important role in keeping the MNRs nucleation and growth.

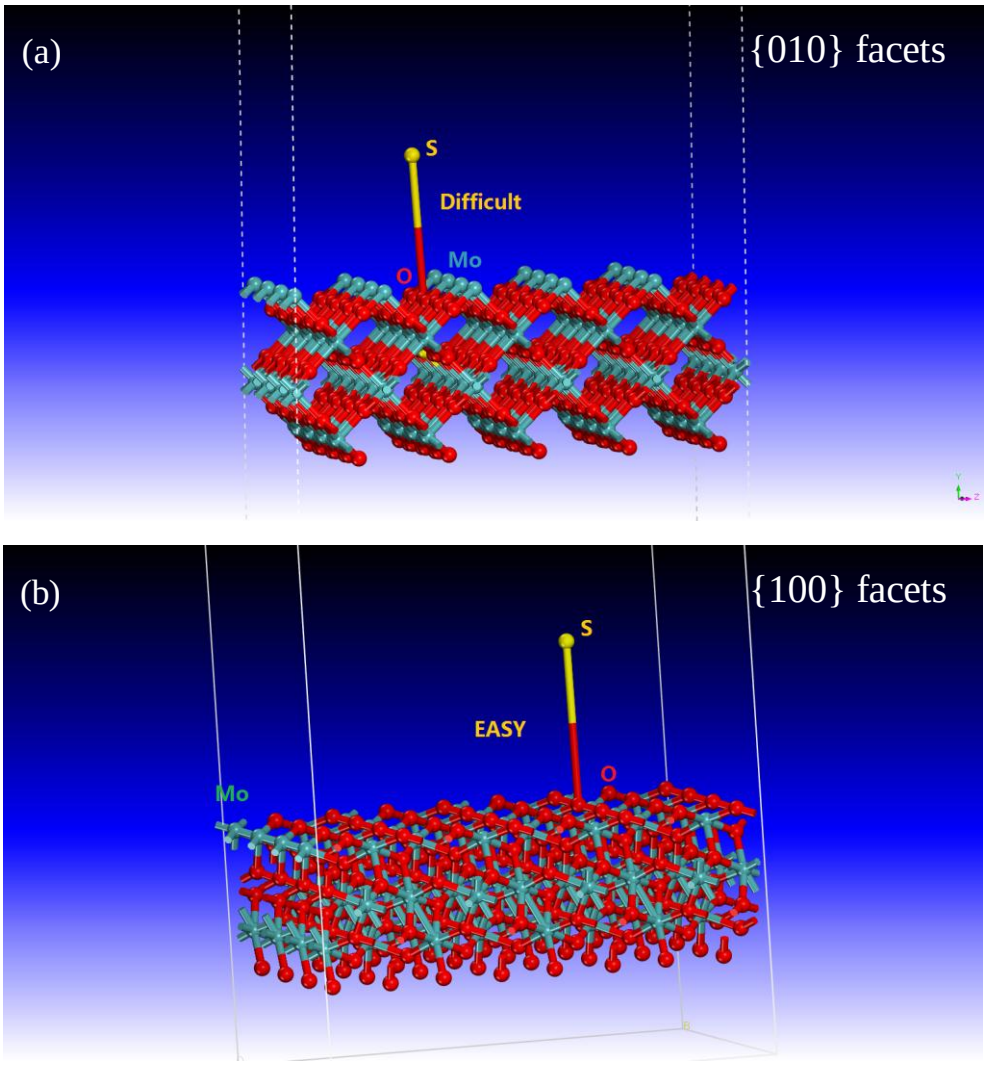

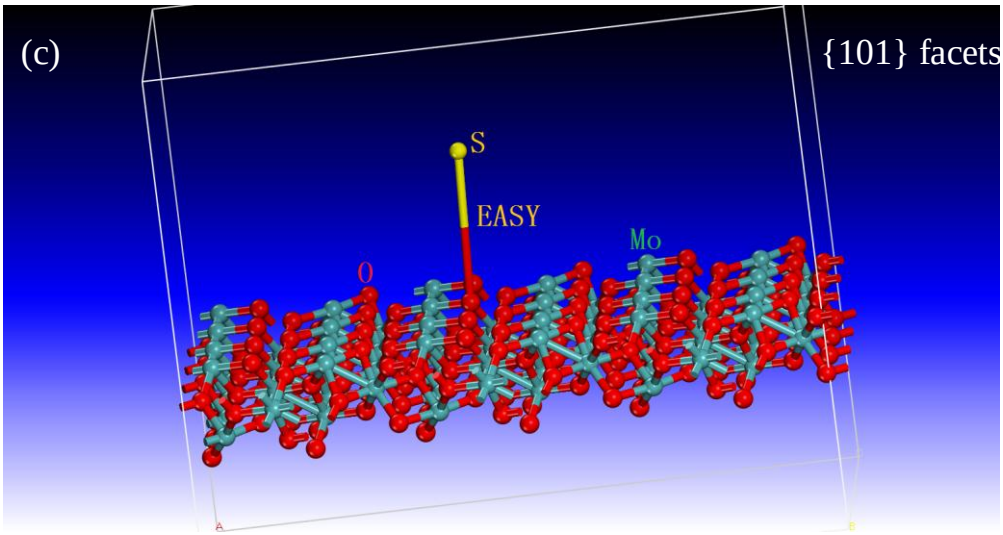

Fig. S7 Possibilities of S replacing O in different facets as (a) {010} main surface, (b) {100} facets, and (c) {101} facets

8. The thickness of MNRs@MoO_2

Fig. S8(a-d) show different thickness of MNRs@MoO_2 on the edge facets, suggesting the layer numbers are within 10 layers. Fig. S8 (e-f) the MNRs@MoO_2 can be exfoliated from its MoO_2 substrate by ultrasonic for 30 min in aqueous solution, and some of the MNRs@MoO_2 stretched out as a perfect single crystal nanoribbons, around 20 nm.

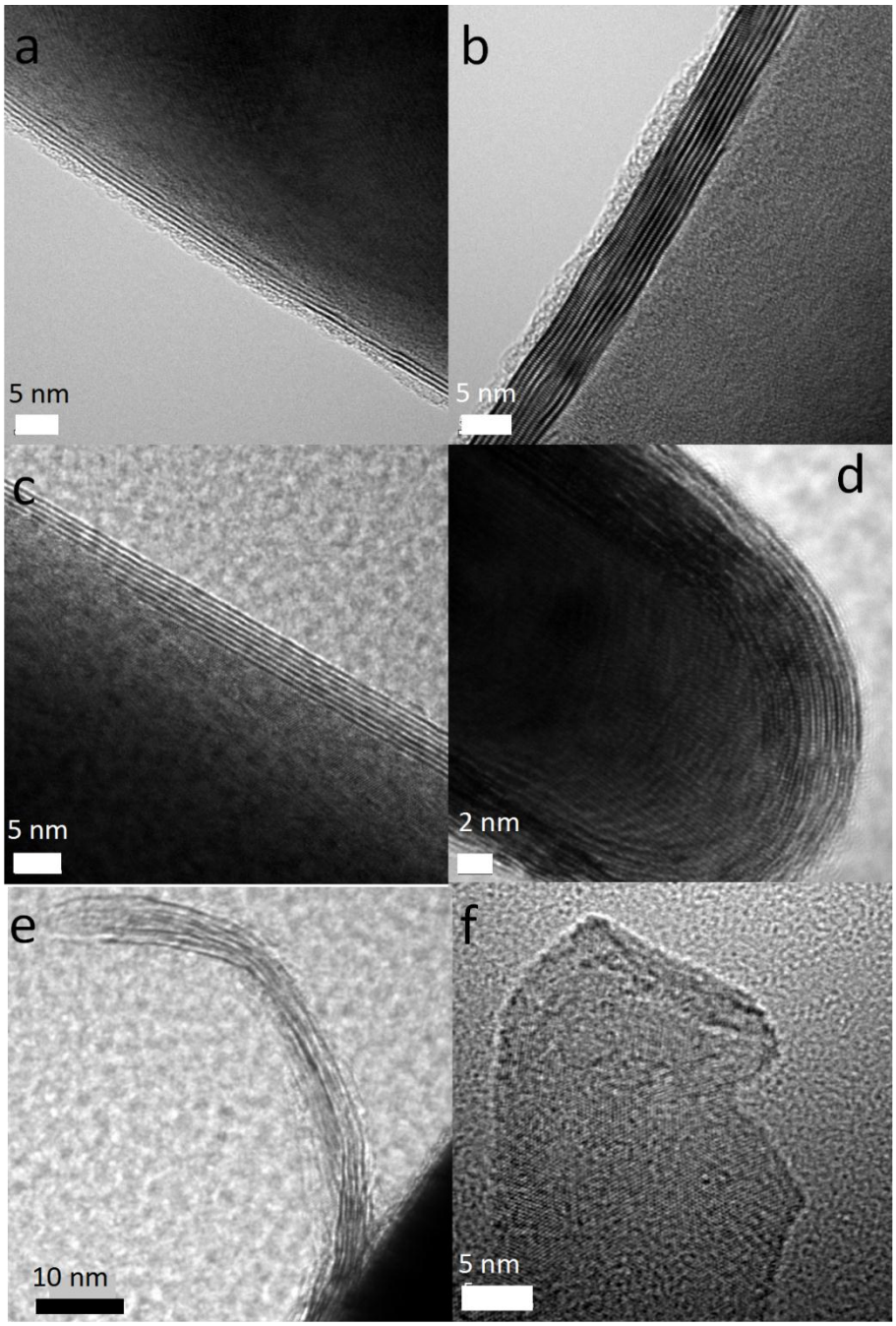

Fig. S8 (a) - (d) Different morphology of MNRs@MoO_2 (AL-750). (e)(f) TEM image of the MNRs@MoO_2 (AL-750) after ultrasonic stripping.

9. The EDS mappingof MNRs@MoO_2

We performed the suggested EDS mapping via HRTEM (Bruker super-XEDS). Since the EDS Kα edge profile of S element are almost identical to Lα edge profile of Mo element, the distribution of the S element cannot be identified from Mo element by EDS mapping.

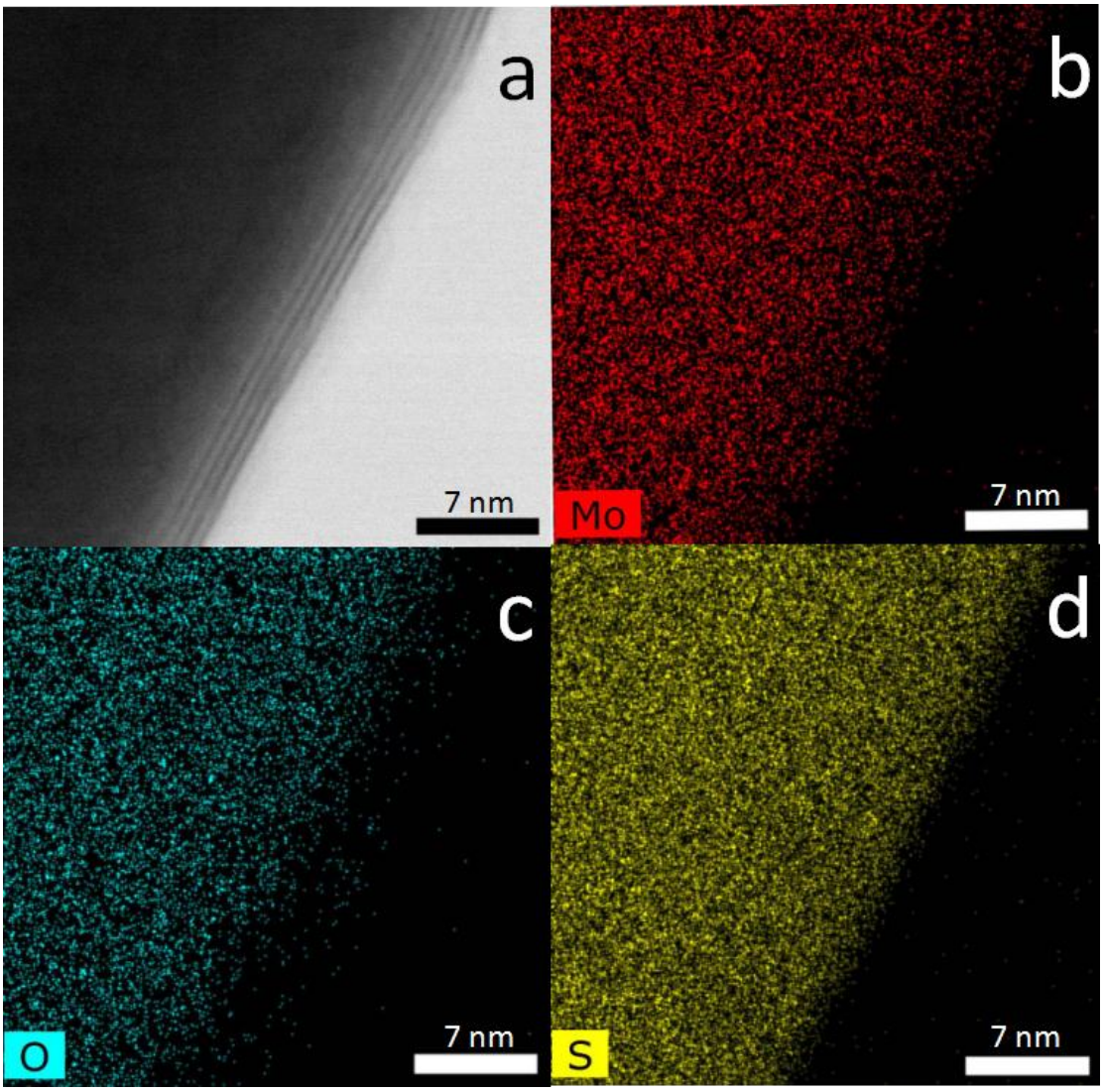

Fig.S9 The EDS Mapping of MNRs@MoO_2 structures. (a) HRTEM image. (b)-(d) EDS mapping for elements of Mo, O, and S respectively.

10. The widthof MNRs@MoO_2

After annealing at 500 ℃, the molybdenum dioxide could be prepared at the cost of the substrate of raw material MoO_3. The freshly obtained molybdenum dioxide nanosheets are perpendicular to the raw MoO_3 surface (Fig. S10(a)). Fig. S10(b-c) show the thickness of newly-born MoO_2. Most of the MoO_2 plates are limited within 100 nm in thickness, resulting in the MNRs width less than 100 nm as well.

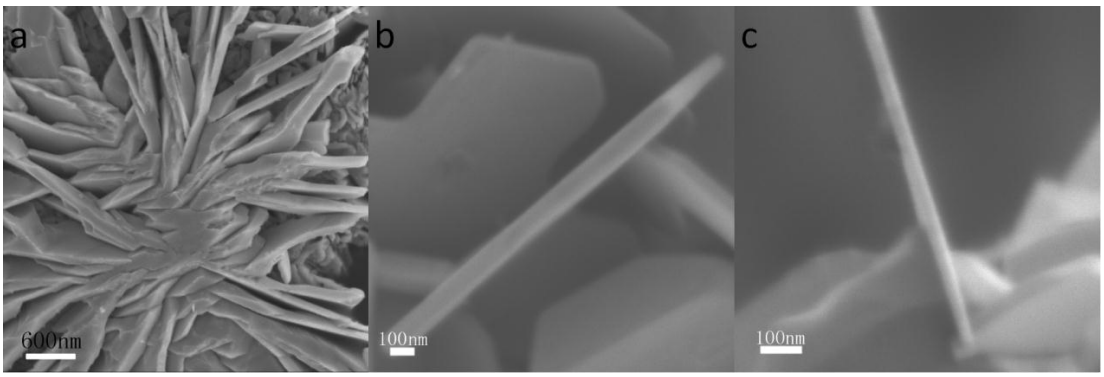

Fig. S10(a) SEM images of the MoS_2@MoO_2, (b-c) show SEM images of different morphologies of MNRs@MoO_2 (AL-750).

11. XRD for MNRs growth process

Figure S11 is XRD spectra of the as-received raw material of MoO_3 (as-received), MoS_2@MoO_2 (AL-500), final product MNRs@MoO_2 (AL-750) and MNRs@MoO_2 (AL-1000). Fig. S11 (a) shows the XRD pattern of the molybdenum trioxide, where all the peaks of pattern are absolutely consistent with XRD card (PDF # 05-0508) of pure α-molybdenum oxide. The specific peak positions are also indexed. Fig. S11 (b) is an XRD pattern of the molybdenum oxide, referring to the XRD cards of molybdenum dioxide (PDF # 78-1069). Residual molybdenum trioxide peak could be found, consistent with the XRD card (PDF # 05-0508), while no peak corresponding to molybdenum disulfide was found. Fig. S11 (c) is the XRD pattern of the product MNRs@MoO_2. Peaks to (002) and (004) of molybdenum disulfide were found (PDF # 87-2416). Fig. S11 (d) shows the XRD pattern of the reference sample synthesized under 1000 ^{o}C (the temperature of the second step is increased to 1000 degrees Celsius), and the pattern conforms to XRD card of molybdenum dioxide (PDF # 78-1069). No peak is consistent with MoO_3 (as-received), indicating molybdenum trioxide as well as essentially complete conversion.

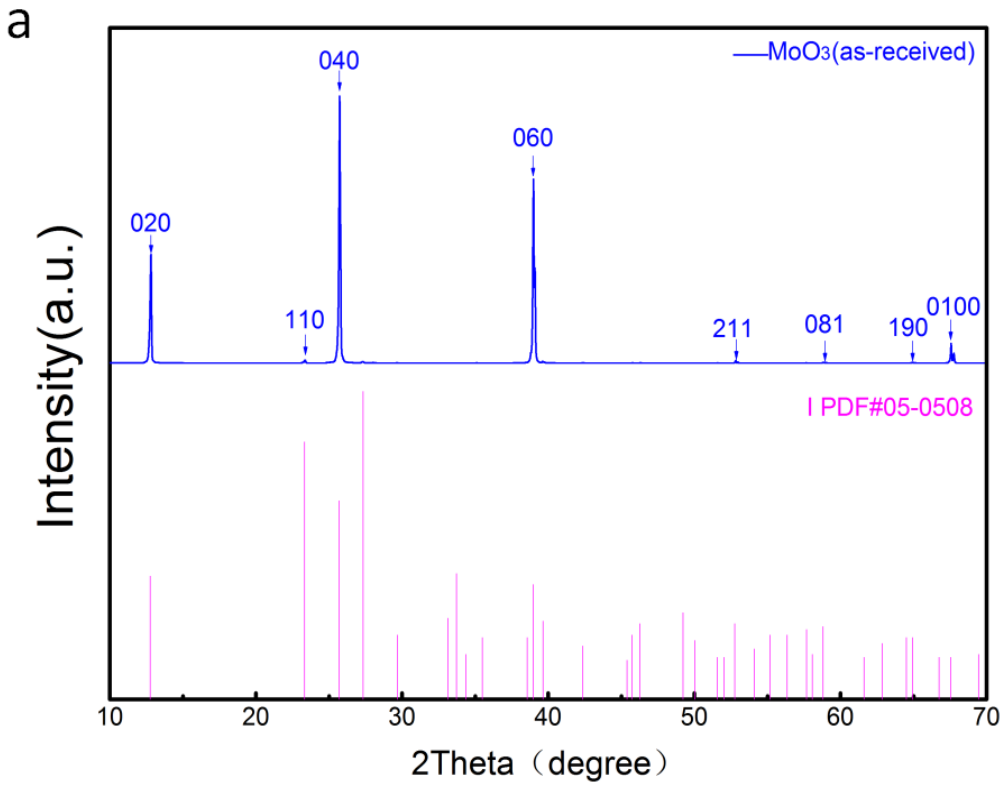
a
MoO3(as-received)
040
060
020
110
211
081
190
0100
I PDF#05-0508
Intensity(a.u.)
10
20
30
40
50
60
70
2Theta（degree）

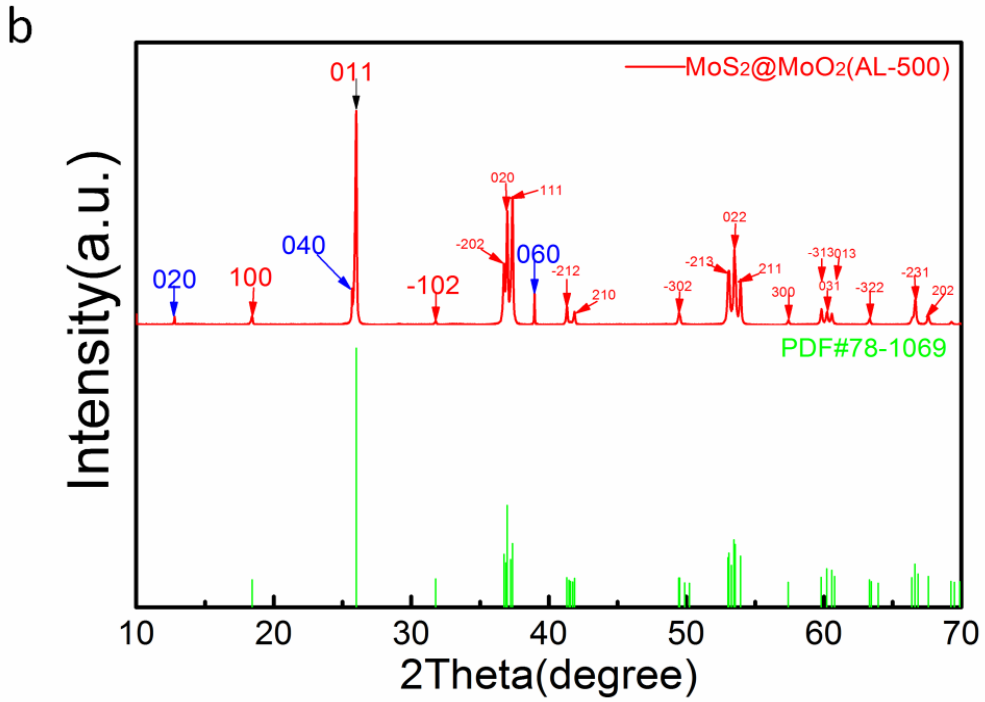
b
MoS2@MoO2(AL-500)
011
020
111
040
060
020
100
-102
-202
-212
210
022
-213
211
-302
300
-313
013
031
-322
-231
202
PDF#78-1069
Intensity(a.u.)
10
20
30
40
50
60
70
2Theta(degree)

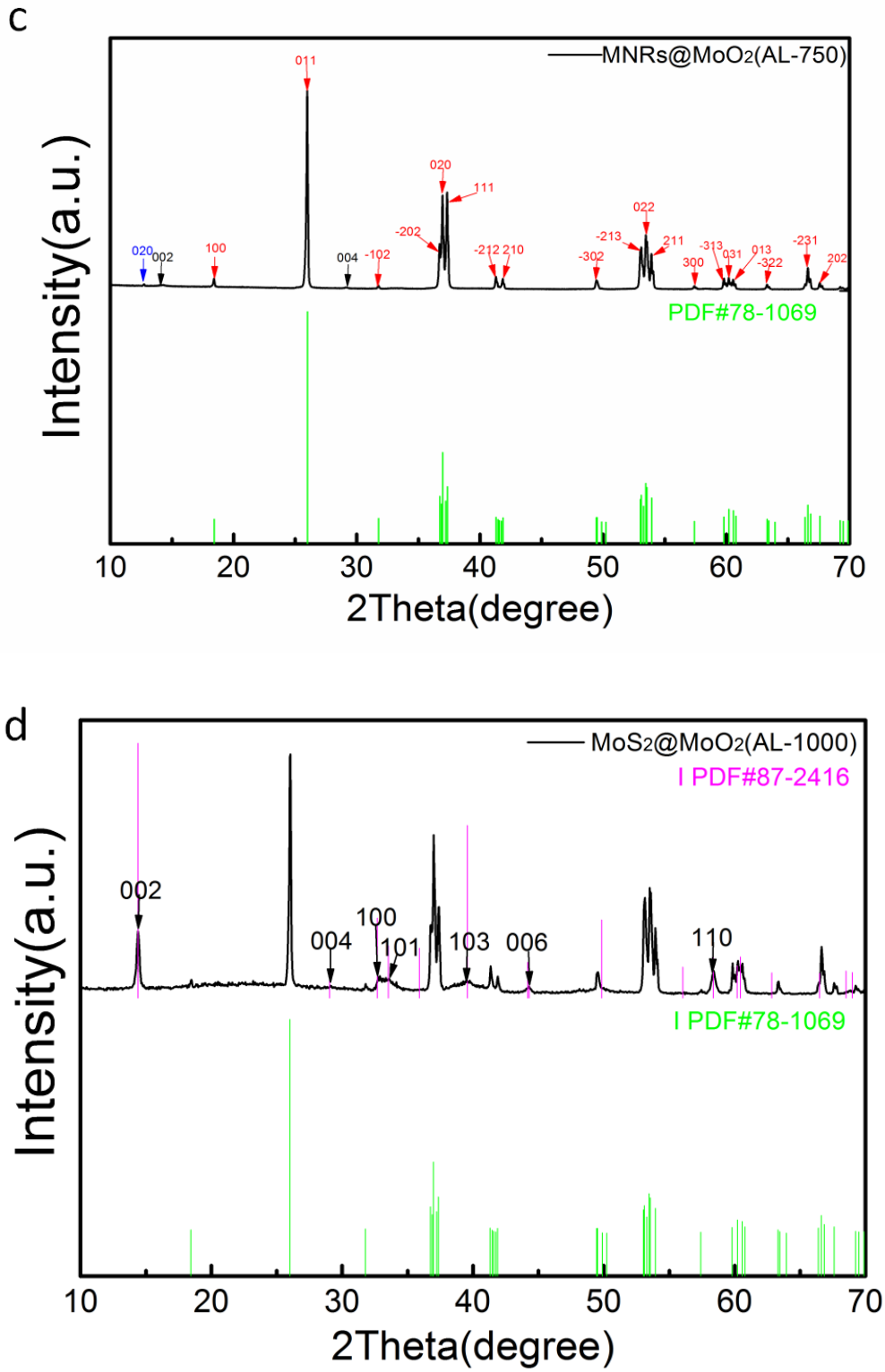

Fig.S11 XRD patterns of (a) MoO_3 (as-received), (b) MoS_2@MoO_2 (AL-500), (c) MNRs@MoO_2 (AL-750), (d) the reference sample MNRs@MoO_2 (AL-1000).

12. XPS for MNRs growth process

The X-ray photoelectron spectroscopy (XPS) shows a same evolutionary process as

well. The survey scan show that only Mo, O and S are detected (Fig. S12(c)). Fig. S12(a) depicts the Mo 3d energy level, offering regular pattern of the pristine the MoO_3, the MoO_2, as well as the MNRs@MoO_2. The energy level of Mo $3d_{5/2}$ suffers a large blue shift, when the MoO_3 was reduced at 500 ^oC for 30 min into MoO_2 (Fig. S12 (a) AL-500 spectrum). The indicative energy level of MoO_3, Mo $3d_{3/2}$, is still survival, suggesting residue MoO_3 in the MoO_2 substrate[4]. After AL-750 process (Fig. S12 (a)), the intensity of Mo $3d_{3/2}$ of MoO_3 become weaker than that by AL-500. The intensity ratio of Mo $3d_{5/2}$ to Mo $3d_{3/2}$ is increased from less than 1 to larger than 1, indicating the MNRs layers increase from 1ML or 2ML to multilayer[5-7]. Fig. S12 (b) illustrates the sulfur 2p energy level, offering a further confirmation of the evolution process complying with the Raman and TEM observations. The peak position of the sulfur 3p after AL-750 mimics that by AL-500, implying no intermediate phase available, e.g. $Mo_xS_yO_z$[6,8-10].

As shown in Fig.S12(c), it is the XPS full-spectrum of MoO_3 (as-received), MoS_2@MoO_2 (AL-500), final product MNRs@MoO_2 (AL-750). The sulfur element appeared after annealing under 500^oC, and Mo3d peak position changed with the reaction proceeding, indicating that the sulfur element is involved in the reaction.

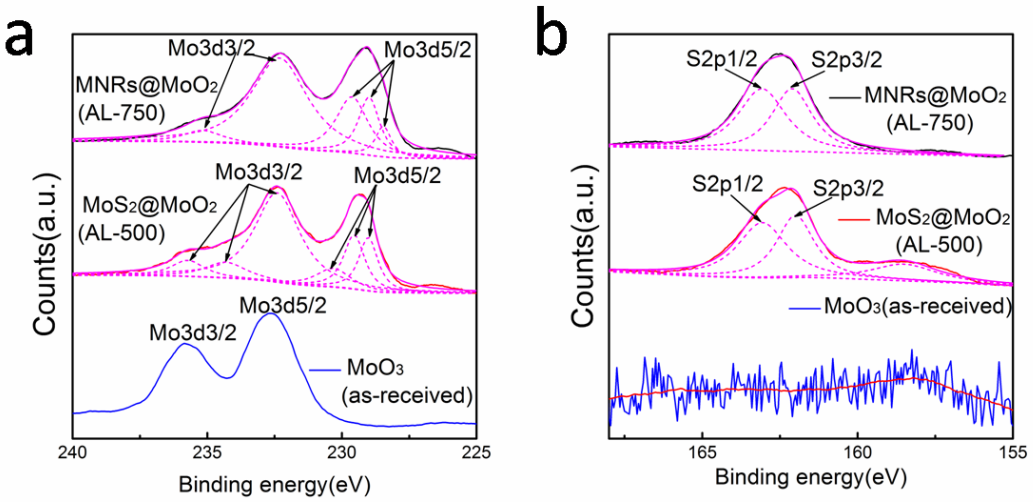

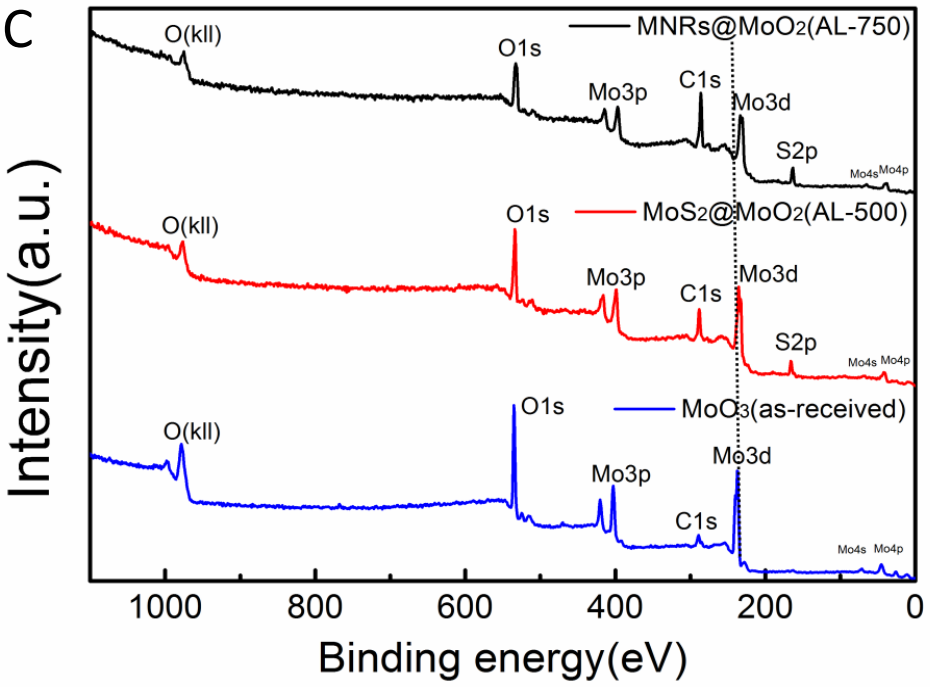

Fig.S12 (a) XPS images of molybdenum atoms and (b) sulfur atoms also proves that the components of three samples.(c)XPS full-spectrum images of the MoO_3 (as-received), MoS_2@MoO_2 (AL-500), MNRs@MoO_2 (AL-750).

13. Simplified bandstructure images of the single-layermolybdenum disulfide

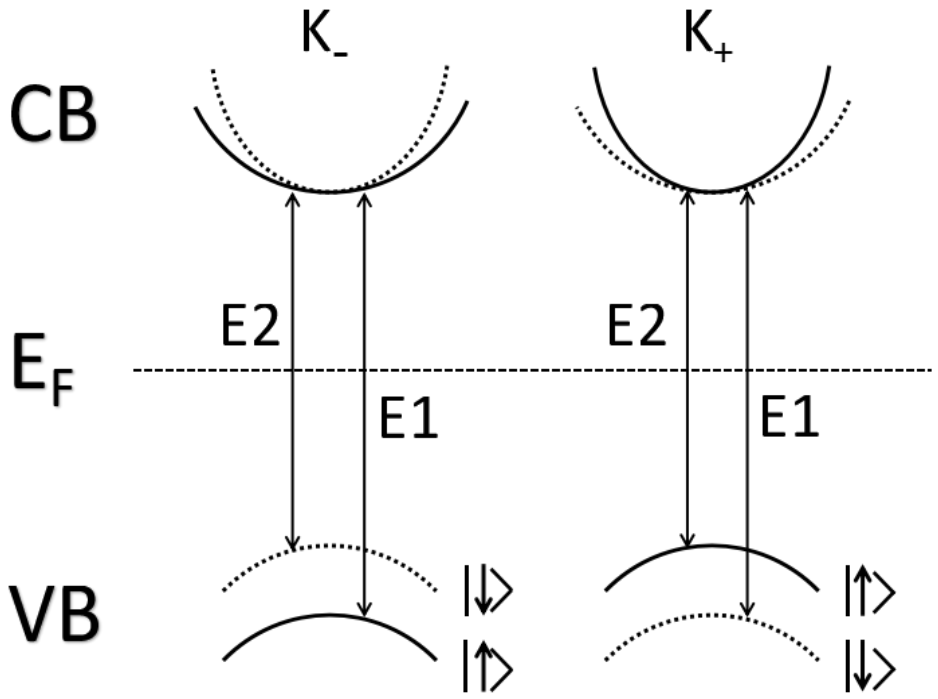

Fig.S13 simplified band structure at the K point of the Brillouin zone for the molybdenum disulfide nanoribbons[11].

14. PL images of different excitation light of the molybdenum disulfide nanoribbons

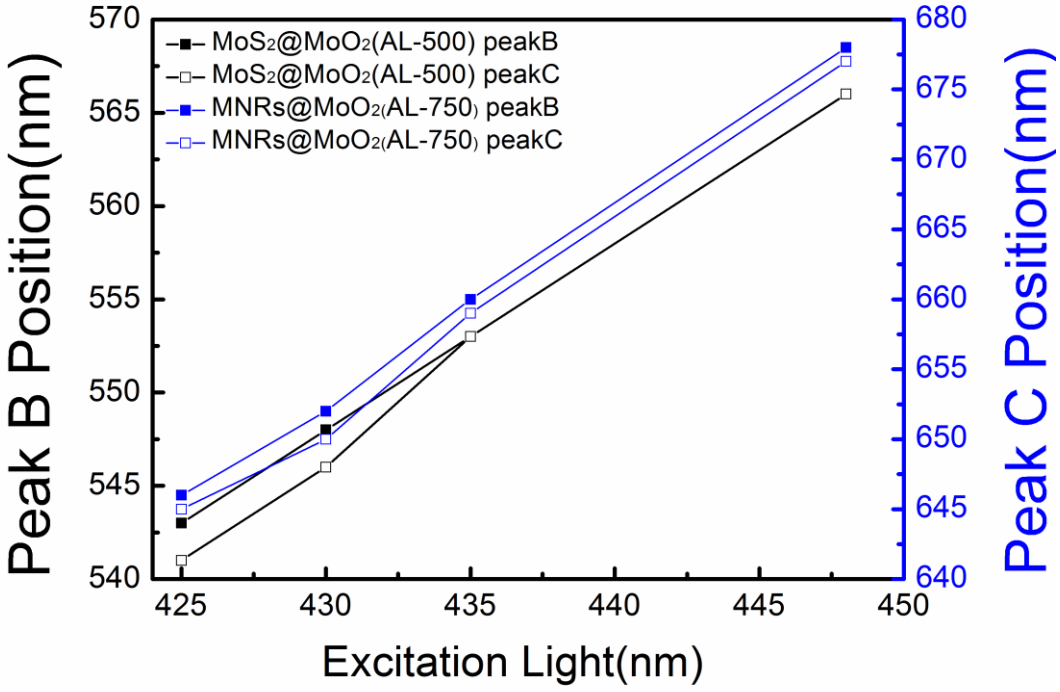

Fig. S14 Peak B and peak C positions excite by different excitation light.

15. MNRs@MoO_2 with Zigzag edge

We performed a HRTEM characterization (FEI titan themis200TEM). With the transmission electron aberration-corrected microscope, the MNRs on the side facets and the templates can be clarified. Fig. S15(a) shows the MNRs@MoO_2 structure. The red frame area was selected randomly. In comparison with the simulated structures of armchair edge (Fig. S15(b))and zigzag edge (Fig. S15(c))[12-15], viewing them from normal directions, the enlarged image of red frame (Fig. S15(d))[15], viewing from the same direction, can be marked with atom positions as Fig. S15(e). As a result, it is very interesting that the edge of our MNRs conforming to the zigzag very well.

In addition, some simulation works have also mentioned the armchair and zigzag edge topologies, viewing side edges from a normal direction, which is in consistent with our researches.

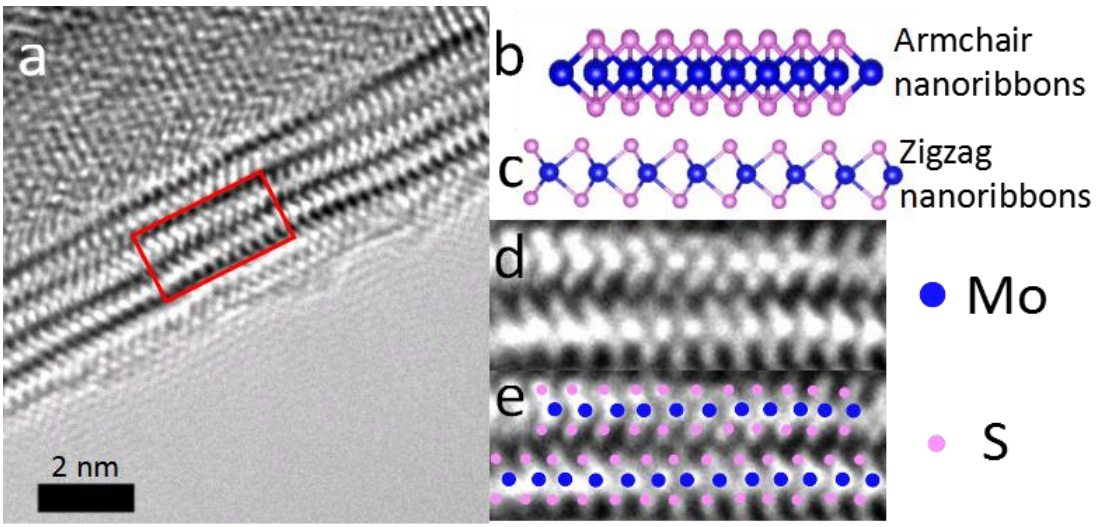

Fig. S15 The transmission electron aberration-corrected microscope of MNRs (a) the MoS_2 nanoribbons epitaxially growing along the side surface of the MoO_2 templates, and the red frame marking the selected area for chirality checking. (b) Schematics of the typical topologies for viewing the armchair side and (c) zigzag side from normal direction. (d) Viewing the MNRs from the top side, and (e) Marking the position of the Mo atoms and S atoms.

16. Schematic diagram for the process of MoS_2 domains extending to the bare edge surface to MNRs

Fig.S16 shows schematic of the molybdenum disulfide nanoribbons. After the MNRs are annealed under 750 ^{o}C, the layer number of the MoS_2 increases from 1 ML to multilayers , as well as the MNRs extends to the bare edge facets of substrate MoO_2 plates, resulting in the proportions of transition zone (heterojunction) increasing.

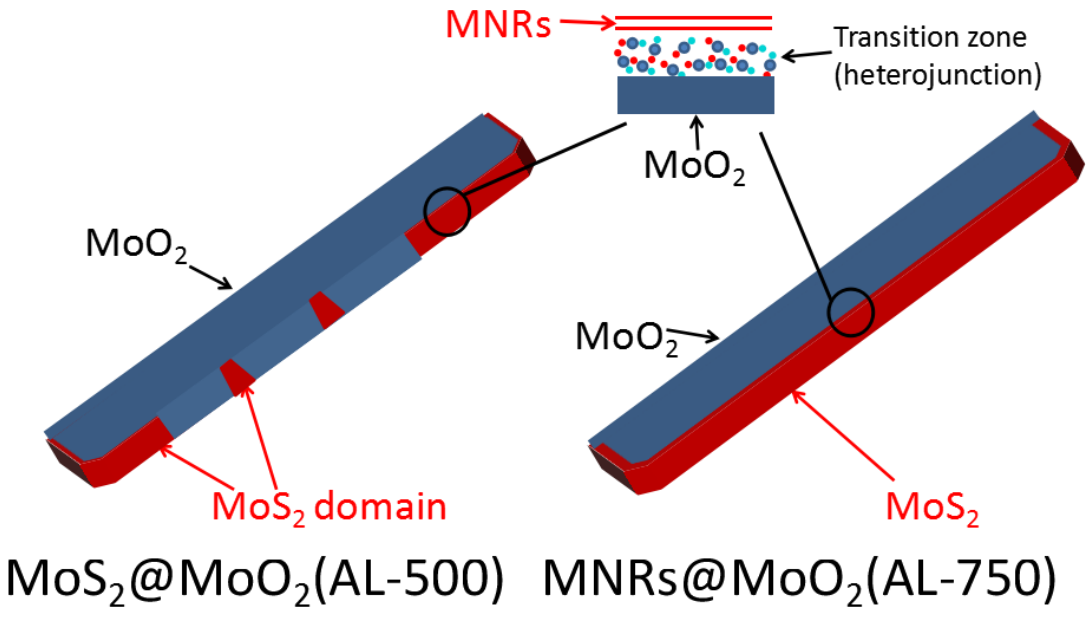

Fig. S16 Schematic diagram images of the molybdenum disulfide nanoribbons

References

1. C. Lee, H. Yan, L. E. Brus, T. F. Heinz, J. Hone and S. Ryu, *ACS nano*, 2010, **4**, 2695-2700.
2. I. Song, C. Park and H. Choi, *Rsc Advances*, 2015, **5**, 7495-7514.
3. B. C. Windom, W. G. Sawyer and D. W. Hahn, *Tribology Letters*, 2011, **42**, 301-310.
4. O. Lupan, V. Cretu, M. Deng, D. Gedamu, I. Paulowicz, S. Kaps, Y. K. Mishra, O. Polonskyi, C. Zamponi and L. Kienle, *Journal of Physical Chemistry C*, 2014, **118**, 15068–15078.
5. Z. Hu, G. Liu, X. Chen, Z. Shen and J. C. Yu, *Advanced Functional Materials*, 2016, **26**, 4445-4455
6. X. Xie, R. Yu, N. Xue, A. B. Yousaf, H. Du, K. Liang, N. Jiang and A.-W. Xu, *Journal of Materials Chemistry A*, 2016, **4**, 1647-1652.
7. M. Acerce, D. Voiry and M. Chhowalla, *Nature nanotechnology*, 2015, **10**, 313.
8. Y. Yang, H. Fei, G. Ruan, C. Xiang and J. M. Tour, *Advanced materials*, 2014, **26**, 8163.
9. W. Wei, L. Samad, J. W. Choi, Y. Joo, A. Way, M. S. Arnold, S. Jin and P. Gopalan, *Chemistry of Materials*, 2016, **28**.
10. G. Eda, H. Yamaguchi, D. Voiry, T. Fujita, M. Chen and M. Chhowalla, *Nano letters*, 2011, **11**, 5111.
11. D. Xiao, G. B. Liu, W. Feng, X. Xu and W. Yao, *Physical review letters*, 2012, **108**, 196802.
12. H. Pan and Y. W. Zhang, *Journal of Physical Chemistry C*, 2012, **116**, 11752-11757.
13. Y. Li, Z. Zhou, S. Zhang and Z. Chen, *Journal of the American Chemical Society*, 2008, **130**, 16739.
14. H. Pan and Y. W. Zhang, *Journal of Materials Chemistry*, 2012, **22**, 7280-7290.
15. Z. Wang, H. Li, Z. Liu, Z. Shi, J. Lu, K. Suenaga, S. K. Joung, T. Okazaki, Z. Gu and J. Zhou, *Journal of the American Chemical Society*, 2010, **132**, 13840-13847.